Journal of the Ceramic Society of Japan 132 [7] 409-414 2024
DOI https://doi.org/10.2109/jcersj2.24026

JCS-Japan

FULL PAPER

# Calcium ion conduction anisotropy of *b*-axis-aligned $CaAl_4O_7$ polycrystal

**Koichiro Fukuda[1,†], Fumiya Nakajima[1], Daisuke Urushihara[1], Toru Asaka[1], Tohru S. Suzuki[2], Abid Berghout[3], Assil Bouzid[3], Olivier Masson[3] and Philippe Thomas[3]**

[1] Division of Advanced Ceramics, Nagoya Institute of Technology, Nagoya 466–8555, Japan
[2] Optical Ceramics Group, Research Center for Electronic and Optical Materials, National Institute for Materials Science, Tsukuba 305–0047, Japan
[3] Université de Limoges, IRCER, CNRS, UMR 7315, 12 Rue Atlantis, F-87000 Limoges, France

**To investigate the anisotropy of $Ca^{2+}$ conduction, the *b*-axis-aligned $CaAl_4O_7$ (space group $C2/c$) polycrystal was prepared by colloidal processing under high magnetic field of 12 T followed by sintering at 1773 K for 2 h. The textured polycrystal was characterized by X-ray diffractometry and impedance spectroscopy with respect to the grain alignment direction, which was parallel to the applied magnetic field. The texture fraction of {0*k*0}, expressed as the Lotgering factor $f_{0k0}$, was 0.63. The ⟨101⟩ directions of individual crystal grains were randomly distributed around the grain-alignment direction of the polycrystal. The conductivities perpendicular ($\sigma_\perp$) and parallel ($\sigma_\parallel$) to the grain alignment direction were compared with the conductivity ($\sigma_{random}$) of random grain oriented polycrystal between 773 and 1073 K. The $\sigma_\perp$, ranging from $3.09 \times 10^{-7}$ to $1.80 \times 10^{-5}$ S cm$^{-1}$, showed the highest value at each temperature, followed by $\sigma_{random}$ and $\sigma_\parallel$ in that order. The results have confirmed for the first time the anisotropy of $Ca^{2+}$ conduction and strongly supported the preferential conduction in the ⟨101⟩ direction predicted in the literature by the bond valence method.**

Key-words : Calcium ion conductor, Grossite, Grain alignment, Anisotropy, Impedance spectroscopy

[Received March 18, 2024; Accepted April 16, 2024; Published online May 18, 2024]

## 1. Introduction

Solid electrolytes with fast conduction of multivalent cations are expected to be used in high performance electrochemical devices such as high capacity rechargeable batteries due to their ability to achieve high density charge transfer.[1)–5)] The solid electrolytes are broadly divided into solid polymer electrolytes and inorganic (ceramic) electrolytes. Since polymer electrolytes have relatively low operating temperatures, their application in rechargeable batteries operating at room temperature has been actively investigated.[6),7)] For ceramic electrolytes, one of the conditions limiting their practical application is their relatively high operating temperatures. They could therefore be used as high-performance energy storage batteries to replace sodium-sulfur batteries in practical use,[8)] which currently operate at 573 K. However, it is generally very difficult for multivalent cations in inorganic crystals to conduct rapidly through the crystal structures due to strong electrostatic interactions with neighboring anions. In view of this situation, Fukuda et al. speculated that in crystals with rigid framework structures and strong structural anisotropy, multivalent cations may conduct relatively easily in specific crystallographic one-dimensional directions.[9)] Using the bond valence (BV) method,[10)–13)] they explored candidate materials based on this hypothesis and found that compounds of the grossite ($CaAl_4O_7$, space group $C2/c$) type may exhibit relatively high $Ca^{2+}$ conductivity in the ⟨101⟩ one-dimensional direction.[9)] The $Ca^{2+}$ conductivity of the random grain oriented $CaAl_4O_7$ polycrystal was superior to that of the NASICON-type $CaZr_4(PO_4)_6$ polycrystal, in which $Ca^{2+}$ conducts three-dimensionally in the crystal structure.[14)] The transference number of $Ca^{2+}$ conduction in $CaAl_4O_7$ was close to 1 at 0.973, indicating almost no electronic or oxide-ion conductivity.[9)] Since calcium is abundant on earth (Clarke number 3.39 %) and has a standard electrode potential value ($Ca^{2+}$/Ca −2.87 V) comparable to that of Li ($Li^+$/Li −3.05 V), fast $Ca^{2+}$ conductors have attracted attention as promising electrolytes for calcium ion-based batteries.[15)]

The crystal grains of ceramics produced by conventional methods tend to have a random orientation. Therefore, even if each individual grain has anisotropic physical and/or mechanical properties, these are cancelled out as a whole and the sintered body exhibits isotropic properties. On the other hand, if the individual grains can be aligned in a particular crystallographic orientation, a significant improvement in properties can be achieved. Conversely, if the intrinsic properties of polycrystals become apparent

† Corresponding author: K. Fukuda; E-mail: fukuda.koichiro@nitech.ac.jp

when the constituent grains are aligned in one direction, this is evidence that they have anisotropic properties. Various methods such as templated grain growth,[16),17)] hot forging,[18)] and reactive diffusion[19)] have been used to orient the constituent crystal grains in ceramics. Recently, it has been reported that single crystal particles of feeble-magnetic materials with very low magnetic susceptibility, such as diamagnetic and paramagnetic materials, can rotate in a strong magnetic field generated by superconducting magnets due to the magnetic torque caused by the magnetic anisotropy of the crystal.[20)–22)] Taking advantage of this phenomenon, Suzuki et al. have successfully produced textured feeble magnetic ceramics by colloidal processing under a strong magnetic field followed by sintering.[21),22)] In general, this method has the advantage that the orientation direction of the particles relative to the sample geometry can be controlled by the direction of the static magnetic field.

In this study, the $Ca^{2+}$ conduction anisotropy of $CaAl_4O_7$ has been experimentally demonstrated for the first time for the *b*-axis-aligned polycrystal, where the direction of grain alignment was perpendicular to the ⟨101⟩ conduction direction predicted by the BV method. If the polycrystals with highly oriented grains in the ⟨101⟩ direction can be produced, a further improvement in conductivity would be expected.

## 2. Experimental

### 2.1 Materials

A well-mixed powder with a [Ca:Al] molar ratio of [1:4] was prepared from the reagent grade chemicals $CaCO_3$ (99.5 %, Kishida Kasei, Osaka, Japan) and $Al_2O_3$ (99.0 %, Kishida Kasei, Japan). It was heated at 1673 K for 5 h and then quenched in air. The heating process was repeated twice with intermediate grinding. The reaction product was a lightly sintered polycrystalline material consisting of $CaAl_4O_7$. The polycrystal was ground in a planetary ball mill (200 rpm, 6 h) to obtain the fine powder, which was dispersed by mutual electrostatic repulsion in distilled water with an appropriate amount of polymeric dispersant. A magnetic field of 12 T was statically applied to the well dispersed suspension during slip casting in the field direction parallel to the casting direction. As it is difficult to rotate diamagnetic particles even in a strong magnetic field, the colloidal processing was used to facilitate the rotation of the particles. Details of the high magnetic field apparatus and the preparation procedure of the suspension are described in the literature.[21)] The crystal particles of $CaAl_4O_7$ were indeed oriented, suggesting that $CaAl_4O_7$ is not non-magnetic but, like $Al_2O_3$, diamagnetic.[22)] The resulting green body was then heated at 1773 K for 2 h in the absence of the magnetic field to prepare the cylindrical sintered polycrystal ($\varphi$11.7 mm and 3.7 mm thick), with the table plane perpendicular to the direction of the applied magnetic field [Fig. S1(a)].

### 2.2 X-ray diffractometry and thermal etching

The resulting sintered polycrystal was cut perpendicular to the table plane using a diamond saw to make two pieces [Fig. S1(b)]. The Cu $K\alpha_1$ beam was incident on the table plane as well as the cross-sectional surface to obtain the X-ray diffraction (XRD) patterns in the Bragg-Brentano geometry using a diffractometer (X'Pert PRO Alpha-1, PANalytical B.V., Almelo, The Netherlands). The integrated reflection intensities were extracted by the Le Bail method[23)] using a computer program RIETAN-FP.[24)] This program was used to generate simulated XRD patterns of polycrystals with random grain orientation and a highly oriented *b*-axis, based on the structural parameters of $CaAl_4O_7$ as determined by Goodwin and Lindop.[25)] The Lotgering factor ($f_{0k0}$),[26)] corresponding to the texture fraction of the {0*k*0} planes, was determined from the *hkl* reflection intensities of the textured polycrystal and those simulated for the randomly grain oriented one.

The cross-sectional surface of one of the cut samples was polished with diamond paste and thermally etched by heating at 1473 K for 0.5 h followed by cooling in air. The thermally etched microtexture was observed using a reflected light microscope.

### 2.3 Impedance spectroscopy

The remaining cut sample was divided into two pieces using the diamond saw. One piece was mechanically polished perpendicular to the original table plane using SiC abrasive paper to prepare the thin plate electrolyte with a thickness ($L$) of 0.241 cm and a surface area ($S$) of 0.302 $cm^2$, giving a shape factor ($L/S$) of $7.98 \times 10^{-1}$ $cm^{-1}$. The resulting electrolyte was designated **1**. The other piece was polished parallel to the original table plane to make the thin plate electrolyte (designated **2**) with $L/S = 5.29 \times 10^{-1}$ $cm^{-1}$ ($L = 0.110$ cm and $S = 0.208$ $cm^2$). Plate electrodes were prepared by applying platinum paste to both sides of electrolytes **1** and **2**, and then heating at 1273 K to decompose the paste and harden the platinum residue. The platinum electrodes fabricated with the present platinum paste were the same as those used in a previous study,[9)] which did not react with the $CaAl_4O_7$ electrolyte at 1073 K. Complex impedance data were collected using an impedance analyzer (IM3570, HIOKI E. E. Co., Nagano, Japan) at temperatures from 773 to 1073 K over the frequency range of 4 to 5 MHz in air. The impedance spectra were analyzed by a distribution of relaxation times (DRT) analysis method using Z-ASSIST software,[27)] followed by a non-linear least squares fitting method using ZView software.[28)] In the adopted equivalent circuit, the elements corresponding to bulk and grain boundary (gb) are connected in series as $(R_{bulk}Q_{bulk})(R_{gb}Q_{gb})$, where $R$ is the resistance in parallel with the constant phase element $Q$. In general, the geometric capacitance ($C$) values and their possible interpretations are $10^{-12}$–$10^{-11}$ F $cm^{-1}$ for $C_{bulk}$, and $10^{-11}$–$10^{-8}$ F $cm^{-1}$ for $C_{gb}$.[29)–31)] The anisotropy of $Ca^{2+}$ conduction in the polycrystal with respect to the direction of grain alignment was explained by the difference in conductivity between electrolyte **1** and electrolyte **2**, taking also into account the conductivity of random grain oriented polycrystal in the literature.[9)]

### 2.4 Bond valence energy landscape method

The potential conductivity of $Ca^{2+}$ in the crystal structure of $CaAl_4O_7$ was investigated by the bond valence energy landscape (BVEL) method,[32),33)] which links the BV method to the absolute energy scale and allows the activation energy of conduction to be estimated. The conduction paths of ions are generally consistent with the spatial distributions of relatively low BV energies. The BV energy of $Ca^{2+}$ was calculated with a resolution of 0.01 nm/voxel using a computer program PyAbstantia.[34)] The energy isosurfaces were superimposed on the structural model, and both were drawn using VESTA software.[35)]

## 3. Results and discussion

### 3.1 Orientation degree of polycrystal

The thermal etching process effectively produced grooves along the grain boundaries, allowing for easy observation of the external shape of each crystal grain with the optical microscope (**Fig. 1**). The crystal grains of all sizes were randomly distributed, and there was no positional bias in the size of the particles, with a maximum grain diameter of approximately 16.5 µm. Therefore, there was no definite correlation between the grain assembly structure and the direction of the magnetic field applied.

The XRD pattern taken from the table plane of the cylindrical sintered polycrystal showed a significant increase in 0*k*0 ($k = 2$, 4, and 6) reflections [**Fig. 2**(a)]. The $f_{0k0}$ value of 0.63 indicates that, during the slip casting of the dispersed particle suspension, the *b*-axis of each crystal grain tended to align along the statically applied magnetic field parallel to the direction of particle settling. The resulting sintered polycrystal was found to be the polycrystalline material with the majority of the constituent crystal grains oriented almost in the *b*-axis direction. On the other hand, the XRD pattern obtained from the cross-sectional surface of the sintered polycrystal showed that the 0*k*0 reflection had completely disappeared [Fig. 2(b)]. This is consistent with the simulated XRD pattern of the polycrystal with a highly oriented *b*-axis (Fig. S2). It is worth noting that the *a*- and *c*-axes are randomly oriented around the oriented *b*-axis for these XRD patterns.

These results confirmed that the *c*- and *a*-directions of individual crystal grains were randomly distributed around the grain alignment direction, which is parallel to the direction of applied magnetic field. It should be noted that the ⟨101⟩ direction lies in the plane formed by the *c*- and *a*-axes and intersects the *b* axis perpendicularly. As a result, we confirmed that the *b*-axes of the individual crystal grains in the sintered polycrystal were highly oriented perpendicular to the table plane, while the ⟨101⟩ directions of the grains were randomly distributed around the grain alignment direction.

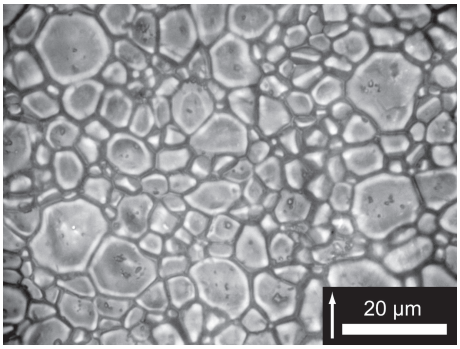


Fig. 1. Thermally etched microtexture produced on the surface parallel to the applied magnetic field as indicated by the white arrow. Reflected light micrograph.

### 3.2 Anisotropy of $Ca^{2+}$ conduction in $CaAl_4O_7$

The Nyquist plot for electrolyte **1** at 773 K showed an incomplete semicircle of bulk contribution, while all other plots for both electrolytes **1** and **2** showed two semicircles with bulk at high frequencies and gb at low frequencies (Figs. S3 and S4). The fitting results and the deconvolution of the two contributions were displayed as blue solid curves and red dashed semicircles, respectively. These two semicircles were well identified as the bulk and gb contributions, since the values of $C_{bulk}$/F cm$^{-1}$ and $C_{gb}$/F cm$^{-1}$ were in good agreement with those determined for ceramic materials.[29)–31)] They were $4.31 \times 10^{-12}$ (873 K)–$5.51 \times 10^{-12}$ (1073 K) for $C_{bulk}$/F cm$^{-1}$ and $4.34 \times 10^{-11}$ (1073 K)–$7.78 \times 10^{-11}$ (873 K) for $C_{gb}$/F cm$^{-1}$ with electrolyte **1**, and $4.10 \times 10^{-12}$ (873 K)–$2.75 \times 10^{-11}$ (773 K) for $C_{bulk}$/F cm$^{-1}$ and $7.56 \times 10^{-11}$ (1073 K)–$3.77 \times 10^{-10}$ (873 K) for $C_{gb}$/F cm$^{-1}$ with electrolyte **2**. The bulk conductivity ($\sigma$) was determined by $1/R_{bulk} \times L/S$.

As the plate electrodes of electrolyte **1** were parallel to the direction of grain alignment, the conductivity determined ($\sigma_\perp$) was in the direction perpendicular to it. The value of $\sigma_\perp$ increased steadily from $3.09 \times 10^{-7}$ to $1.80 \times 10^{-5}$ S cm$^{-1}$ with increasing temperature from 773 to 1073 K (**Fig. 3**). The activation energy of conduction ($E_a$) was 1.060(15) eV. On the other hand, since the plate electrodes of electrolyte **2** were perpendicular to the direction of grain alignment, the obtained conductivity ($\sigma_\parallel$) was in the direction parallel to it. The $\sigma_\parallel$ value also showed the steady increase with increasing temperature from $1.49 \times 10^{-8}$ to $1.99 \times 10^{-6}$ S cm$^{-1}$ over the same temperature range, and the $E_a$ value was 1.22(2) eV (Fig. 3). The ionic conductivity of the random grain oriented polycrystal ($\sigma_{random}$) showed the intermediate value, together with the intermediate activation energy of 1.14(2) eV.[9)] When compared at the same temperatures, the $\sigma_\perp$ value was 9.1 (1073 K) to 20.8 (773 K) times larger than the $\sigma_\parallel$ value. However, when comparing the $\sigma_\perp$ and $\sigma_{random}$ values, the former was only 1.6 (1073 K) to 2.3 (773 K) times larger than the latter, and the difference was not as pronounced. A significant difference was observed between the $\sigma_\parallel$ and $\sigma_{random}$ values, the latter being 5.6 (1073 K) to 9.2 (773 K) times larger than the former. The direction of $Ca^{2+}$ conduction was predicted by the BV method to be parallel to ⟨101⟩,[9)] which intersects perpendicular to the *b*-axis direction in the crystal structure. Accordingly, the conductivity of the *b*-axis-aligned polycrystal is expected to be relatively high for $\sigma_\perp$ and low for $\sigma_\parallel$, and this was indeed the case.

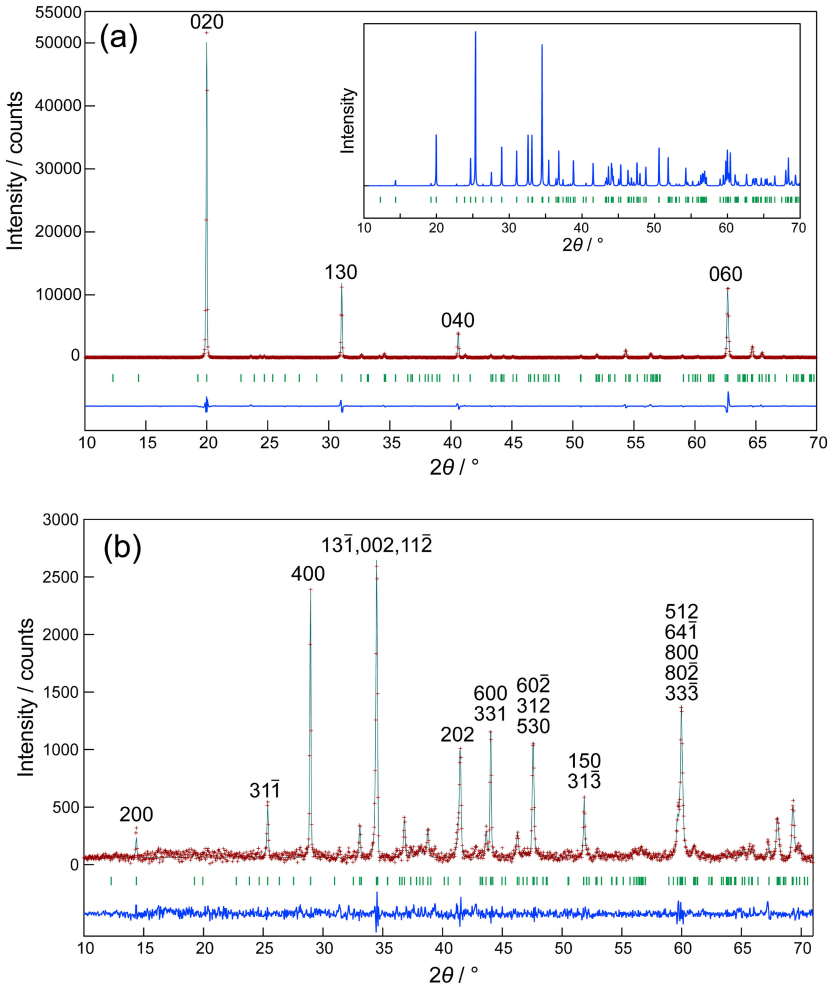


Fig. 2. Fitting results of the observed X-ray diffraction patterns (red symbol: +) of the sintered polycrystal. The irradiated surface areas are perpendicular to the grain alignment direction in (a) and parallel to it in (b). In each diagram, the calculated pattern and the positions of the possible Bragg reflections are indicated by the upper solid line and the lower vertical bars, respectively, and the difference curve is displayed in the lower part of the diagram. Inset in (a): Simulated X-ray diffraction pattern of the random grain oriented $CaAl_4O_7$ polycrystal.

The reason for the larger value of $\sigma_\perp$ than that of $\sigma_{random}$ is due to the larger fraction of ⟨101⟩ aligned crystal grains in the direction in which the ionic conductivity was measured.

Since the semicircles of grain boundary were clearly recognizable in the Nyquist plots at temperatures between 873 and 1073 K for electrolyte **1** (Fig. S3), the grain boundary conductivity was plotted together with the total conductivity in Fig. S5 with an activation energy of 0.70(3) eV for the former conduction. As the grain boundary volume fraction and grain size distribution of polycrystals are expected to influence the grain boundary conductivity, clarification of this relationship is an important subject when considering the practical application of the electrolyte, as it may contribute to improving the overall conductivity.

If the direction of $Ca^{2+}$ conduction were restricted to the ⟨101⟩ one-dimensional direction, the perfectly *b*-axis-aligned $CaAl_4O_7$ polycrystal with $f_{0k0} = 1$ should show no conduction at all in the grain alignment direction. In fact, the conduction was observed in the grain-alignment direction of the textured polycrystal obtained and the $\sigma_\perp$ value was determined by the complex impedance method. There are two possible reasons for this. First, the conduction paths in the $CaAl_4O_7$ crystal exist not only in the ⟨101⟩ direction but also in other directions. Second, although the degree of orientation ($f_{0k0}$) of the grain-aligned polycrystal was as high as 0.63, it was not completely *b*-axis oriented. Thus, within the grain-aligned polycrystal, there would be locations where ⟨101⟩ conduction paths are connected between adjacent grains, forming conduction paths in the direction of grain alignment. We used the BVEL method to verify the first possibility and found new conduction paths along the ⟨001⟩ direction (Fig. S6). The $E_a$ values were derived from the spatial distribution of the BV energy to be 1.59 eV in the ⟨101⟩ direction and 4.36 eV in the ⟨001⟩ direction. It is well known that theoretical $E_a$ values derived from the BVEL method tend to be higher than experimental values, partly because they do not take into account the effects of lattice relaxation associated with ion conduction.[33] Assuming that the $E_a$ value of the former

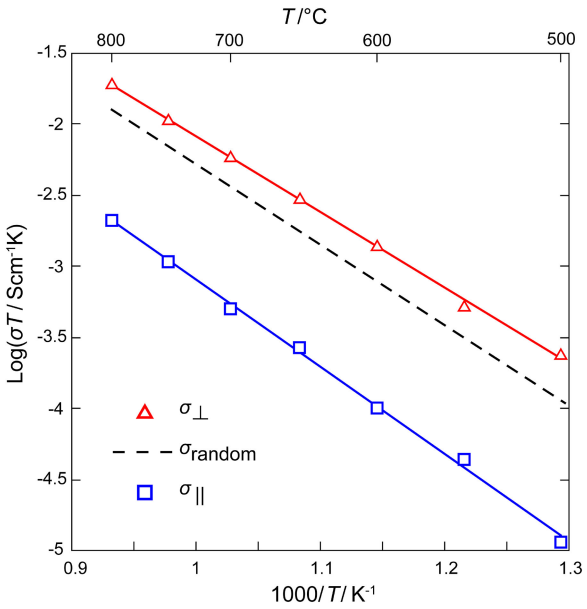


Fig. 3. Anisotropy of $Ca^{2+}$ conduction in *b*-axis-aligned $CaAl_4O_7$ polycrystals. Conductivity $\sigma_\perp$ perpendicular to the direction of grain alignment and conductivity $\sigma_\parallel$ parallel to it. Conductivity $\sigma_{random}$ for random grain oriented polycrystal.[9)]

was the same as that of $\sigma_\perp$ (= 1.06 eV), the latter corrected by the scaling factor of 0.667 (= 1.06/1.59) is 2.91 eV. Thus, the $E_a$ value of $Ca^{2+}$ conduction in the ⟨001⟩ direction would be approximately 2.7 times larger than that in the ⟨101⟩ direction. Whether or not conduction in the ⟨001⟩ direction actually occurs would be verified by, for example, molecular dynamics simulation methods and/or experimental measurements of anisotropic conduction for the single crystals. Since the conduction paths in the ⟨101⟩ and ⟨001⟩ directions are both perpendicular to the *b*-axis, they do not contribute to the conduction in the *b*-axis direction. It is therefore possible that the second reason is the cause.

The possibility of $Ca^{2+}$ conduction in $CaAl_4O_7$ was first demonstrated by the BV method, and subsequently confirmed experimentally for the random grain oriented polycrystal.[9)] However, it was unclear whether the predicted conduction in the ⟨101⟩ direction actually occurs in the crystal structure. In this study, the anisotropy of $Ca^{2+}$ conduction has been experimentally confirmed for the first time, strongly supporting that the conduction direction is mainly along ⟨101⟩. If polycrystals with a higher degree of orientation, preferably in the ⟨101⟩ direction, could be obtained, the $Ca^{2+}$ conductivity would be expected to be higher than that of the present polycrystal.

The elucidation of the $Ca^{2+}$ conduction mechanism would provide another guideline for conductivity enhancement. Whether there are defects in the Ca sites in the crystal structure of $CaAl_4O_7$ and, if so, how their concentrations affect the $Ca^{2+}$ conductivity are important issues closely related to the $Ca^{2+}$ conduction mechanism. The stoichiometric composition of the sample must be accurately determined and its relationship to $Ca^{2+}$ conductivity clarified.

## 4. Conclusion

The polycrystalline $CaAl_4O_7$ (space group $C2/c$) was prepared by colloidal processing under the high magnetic field of 12 T followed by heating at 1773 K for 2 h. During the former process of slip casting the dispersed particle suspension, the *b*-axis of each crystal grain tended to align along the statically applied magnetic field parallel to the direction of particle settling. Thus, after sintering in the absence of the magnetic field, the resulting polycrystal exhibited a high *b*-axis orientation with the Lotgering factor $f_{0k0}$ of 0.63, and the ⟨101⟩ directions of individual crystal grains were randomly distributed around the grain alignment direction. The conductivities perpendicular ($\sigma_\perp$) and parallel ($\sigma_\parallel$) to this direction were compared between 773 and 1073 K, together with the conductivity ($\sigma_{random}$) of random grain oriented polycrystal. The value of $\sigma_\perp$ increased steadily from $3.09 \times 10^{-7}$ to $1.80 \times 10^{-5}$ S cm$^{-1}$ with increasing temperature. When compared at the same temperature, $\sigma_\perp$ had the highest value, followed by $\sigma_{random}$ and then $\sigma_\parallel$ in that order. In this study, the anisotropy of $Ca^{2+}$ conduction in $CaAl_4O_7$ was confirmed for the first time, and the results obtained were consistent with preferential conduction in the ⟨101⟩ direction as predicted by the BV method. If the polycrystals with highly oriented grains in the ⟨101⟩ direction can be produced, a further improvement in conductivity would be expected.

**Appendix A. Supporting information** Supplementary data associated with this article can be found in the on line version.

**Acknowledgment** This research was supported by a Grant-in-Aid for Scientific Research (No. 19K22051) from the Japan Society for the Promotion of Science.

## References

1) L. F. O'Donnell and S. G. Greenbaum, *Batteries*, **7**, 3 (2021).
2) Y. Liang, H. Dong, D. Aurbach and Y. Yao, *Nat. Energy*, **5**, 646–656 (2020).
3) A. Ponrouch, J. Bitenc, R. Dominko, N. Lindahl, P. Johansson and M. R. Palacín, *Energy Storage Mater.*, **20**, 253–262 (2019).
4) N. Imanaka and S. Tamura, *B. Chem. Soc. Jpn.*, **84**, 353–362 (2011).
5) N. Imanaka, *J. Ceram. Soc. Jpn.*, **113**, 387–393 (2005).
6) F. S. Genier, C. V. Burdin, S. Biria and I. D. Hosein, *J. Power Sources*, **414**, 302–307 (2019).
7) Q. Wei, L. Zhang, X. Sun and T. L. Liu, *Chem. Sci.*, **13**, 5797–5812 (2022).
8) D. Kumar, S. K. Rajouria, S. B. Kuhar and D. K. Kanchan, *Solid State Ionics*, **312**, 8–16 (2017).
9) K. Fukuda, R. Harada, H. Banno, D. Urushihara and T. Asaka, *ACS Appl. Energ. Mater.*, **5**, 3227–3234 (2022).
10) S. Adams, K. Hariharan and J. Maier, *Solid State Ionics*, **86–88**, 503–509 (1996).
11) S. Adams and J. Maier, *Solid State Ionics*, **105**, 67–74 (1998).
12) S. Adams, *Solid State Ionics*, **136–137**, 1351–1361

(2000).
13) M. Avdeev, M. Sale, S. Adams and R. Prasada, *Solid State Ionics*, 225, 43–46 (2012).
14) K. Nomura, S. Ikeda, K. Ito and H. Einaga, *B. Chem. Soc. Jpn.*, 65, 3221–3227 (1992).
15) M. E. Arroyo-de Dompablo, A. Ponrouch, P. Johansson and M. R. Palacín, *Chem. Rev.*, 120, 6331–6357 (2020).
16) H. Igarashi, K. Matsunaga, T. Taniai and K. Okazaki, *Am. Ceram. Soc. Bull.*, 57, 815–817 (1978).
17) M. Holmes, R. E. Newnham and L. E. Cross, *Am. Ceram. Soc. Bull.*, 58, 872 (1979).
18) T. Takenaka and K. Sakata, *Jpn. J. Appl. Phys.*, 19, 31–39 (1980).
19) K. Fukuda, T. Asaka, R. Hamaguchi, T. Suzuki, H. Oka, A. Berghout, E. Béchade, O. Masson, I. Julien, E. Champion and P. Thomas, *Chem. Mater.*, 23, 5474–5483 (2011).
20) T. Sugiyama, M. Tahashi, K. Sassa and S. Asai, *ISIJ Int.*, 43, 855–861 (2003).
21) T. S. Suzuki, *J. Ceram. Soc. Jpn.*, 128, 1005–1012 (2020).
22) T. S. Suzuki, T. Uchikoshi and Y. Sakka, *Sci. Technol. Adv. Mat.*, 7, 356–364 (2006).
23) A. Le Bail, H. Duroy and J. L. Fourquet, *Mater. Res. Bull.*, 23, 447–452 (1988).
24) F. Izumi and K. Momma, *Solid State Phenom.*, 130, 15–20 (2007).
25) D. W. Goodwin and A. J. Lindop, *Acta Crystallogr. B*, 26, 1230–1235 (1970).
26) F. K. Lotgering, *J. Inorg. Nucl. Chem.*, 9, 113–123 (1959).
27) H. Sumi, H. Shimada, Y. Yamaguchi, T. Yamaguchi and Y. Fujishiro, *Electrochim. Acta*, 339, 135913 (2020).
28) D. Johnson, ZView Program (Version 2.9b), Scribner Associates Inc., Southern Pines, NC (1990).
29) J. T. S. Irvine, D. C. Sinclair and A. R. West, *Adv. Mater.*, 2, 132–138 (1990).
30) X. Vendrell and A. R. West, *J. Electrochem. Soc.*, 165, F966–F975 (2018).
31) I. N. David, T. Thompson, J. Wolfenstine, J. L. Allen and J. Sakamoto, *J. Am. Ceram. Soc.*, 98, 1209–1214 (2015).
32) S. Adams and R. P. Rao, *Phys. Status Solidi A*, 208, 1746–1753 (2011).
33) S. Adams and R. P. Rao, Understanding Ionic Conduction and Energy Storage Materials with Bond-Valence-Based Methods, in “Bond Valences”, Ed. by I. D. Brown and K. R. Poeppelmeier, Springer, Berlin Heidelberg (2014) pp. 129–159.
34) P. Barpanda, G. Oyama, S. Nishimura, S.-C. Chung and A. Yamada, *Nat. Commun.*, 5, 4358 (2014).
35) K. Momma and F. Izumi, *J. Appl. Crystallogr.*, 44, 1272–1276 (2011).